Semiconductor Physics, Quantum Electronics & Optoelectronics, 2015. V. 18, N 3. P. 267-271.
doi: 10.15407/spqeo18.03.267

PACS 73.40.Kp, 73.40.Gk

Carrier transport mechanisms in reverse biased InSb *p-n* junctions

A.V. Sukach[1], V.V. Tetyorkin[1], A.I. Tkachuk[2]
[1]*V. Lashkaryov Institute of Semiconductor Physics, NAS of Ukraine,*
41, prospect Nauky, 03028 Kyiv, Ukraine
[2]*V. Vinnichenko Kirovograd State Pedagogical University, Kirovograd, Ukraine*
Phone 38 (044) 525-1813, e-mail: teterkin@isp.kiev.ua

Abstract. Carrier transport mechanisms have been investigated in linearly graded InSb *p-n* junctions prepared using thermal diffusion of Cd into single crystal substrates of n-type conductivity. The investigations were focused on the reverse current as a function of bias voltage and temperature. The obtained experimental data show that local inhomogeneities in the depletion region are responsible for the excess tunneling current observed in the reverse biased junctions. The inhomogeneities have been attributed to dislocations, precipitates or other extended defects. A phenomenological model is proposed to explain experimental data.

Keywords: InSb, photodiode, inhomogeneous junction, tunnelling breakdown.

Manuscript received 12.03.15; revised version received 28.05.15; accepted for publication 03.09.15; published online 30.09.15.

1. Introduction

Due to high structural perfection of InSb single crystals, cooled photodiodes based on them are widely used for detection of infrared radiation within the spectral range 3 to 5 μm [1-4]. Despite the fact that technology of InSb photodiodes is improved over the last 40 years [5], a number of problems remain valid [6, 7]. For instance, it is known that IR photodiodes made of narrow-gap semiconductors, including InSb photodiode, suffer from excess leakage current at reverse bias, which can limit their performance. Thus, understanding its nature is of great importance. Experimental results published in literature have contradictory character and suggestions on the nature of the excess current mechanism and are very different. For instance, it was explained by the surface leakage [2] or by tunneling with participation of extended defects (dislocations, precipitates) intersecting the depletion region [8]. In *p-n* junctions produced by ion implantation with Be or Mg, the interband tunneling current was shown to be dominant at high reverse bias voltages [5, 9, 10]. The breakdown voltage, U_B, lies within the range 3 to 5 V. Higher values of the breakdown voltage U_B = 14…30 V associated with the avalanche breakdown mechanism were observed in diffused photodiodes [11, 12]. At last, in photodiodes produced by molecular beam epitaxy the voltage of avalanche gain was 4.5 V [13]. Thus, significant difference in the breakdown voltage in photodiodes produced by different methods, as well as the nature of tunneling current in photodiodes with a rather wide depletion region (approximately 0.5…1.0 μm at 77 K) requires more thorough investigation, which was the purpose of this study.

2. Samples and experimental methods

The investigated *p-n* junctions were produced by diffusion of cadmium into monocrystalline substrates of *n*-type conductivity with crystallographic orientation (100) and average thickness close to 500 μm. The concentration and mobility of electrons in the substrates

© 2015, V. Lashkaryov Institute of Semiconductor Physics, National Academy of Sciences of Ukraine

were of the order of $1.0 \cdot 10^{15}$ cm^{-3} and $5.0 \cdot 10^{5}$ cm^2/V·s at 77 K, respectively. The average density of dislocations (the etching pits density) was less than 350 cm^{-2} [14]. The damaged layer was removed by chemical dynamic polishing using the polishing etchant 2% Br_2 + HBr. The surface quality was controlled by an interference microscope. The measured roughness at the surface after polishing was close to 0.03 μm. Diffusion of dopant was carried in a two-temperature furnace. The substrate and source temperatures were 400 and 380 °C, respectively. To prevent reevaporation of substrate components, additionial amount of InSb and elemental Sb were placed into a silica ampoule to ensure the saturation vapor condition. The junction depth was determined by measuring the sign of thermoEMF by using the probe method during sequential chemical etching of the doped surface layer. The mesa structures with the active area $1.4 \cdot 10^{-2}$ cm^2 and the junction depth close to 3 μm were delineated. As determined by a differential Hall effect [15], the average concentration of holes in the doped layer was $(7\pm1) \cdot 10^{18}$ cm^{-3} at 77 K. Ohmic contacts to *p*- and *n*-type regions of the junctions were prepared using In-Zn alloy and pure In, respectively. Formation of ohmic contacts and purification of mesas has been carried out in a hydrogen atmosphere at approximately 350 °C for 5 to 10 min. Thin polycrystalline films of CdTe were used as passivation and protective layers due to lattice parameters and thermal expansion coefficients of CdTe and InSb agrees well. By using polycrystalline CdTe, the density of interface states in the CdTe-InSb heterojunction can be 3- to 4-fold reduced as compared to the oxide-InSb interface [16]. The current-voltage and high-frequency (1 MHz) capacitance-voltage characteristics were measured as functions of the bias voltage and temperature.

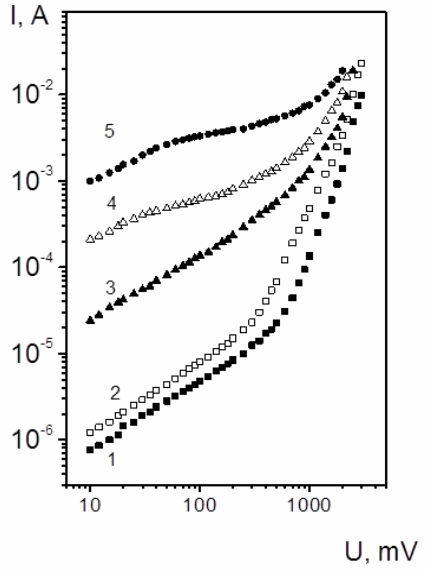

Fig. 1. Reverse *I–U* characteristics of diffused InSb *p-n* junctions at temperatures, K: 77 (*1*), 89 (*2*), 120 (*3*), 138 (*4*), 156 (*5*).

3. Results and discussion

The measured capacitance-voltage characteristics are linearized in C^{-3}–U coordinates indicating formation of linearly graded junctions. Typical values of the concentration gradient $a = 1.0 \cdot 10^{19}$ cm^{-4} and the built-in voltage $U_{bi} = 190$ mV were determined from the slope of C^{-3}–U straight lines and their intersection with the voltage axis, respectively. The depletions region width, W, was estimated as 1.3 μm at 77 K. The *I–U* characteristics within the temperature range 77…160 K are described by the formula:

$$I = I_{01} \exp\left[\frac{e(U - IR_s)}{E_0}\right] + I_{02} \exp\left[\frac{e(U - IR_s)}{\beta KT}\right], \qquad (1)$$

where $E_0 = 29$ meV is the characteristic energy, $\beta = 1.6$ – ideality factor. The series resistance and built-in potential determined from the *I–U* characteristics were 1.4 Ohm and 160 mV, respectively. The discrepancy in experimental values of the built-in potential determined by different methods is caused by the series resistance. The rectification ratio at 77 K is reached 10^3 at voltages ±250 mV. The carrier transport mechanisms in diffused InSb junctions at direct biases were analyzed in details previously [8].

In order to clarify the impact of the surface leakage, the *I–U* characteristics were investigated in a series of junctions with a different ratio of the junction area A to the perimeter length. It was concluded that in the investigated junctions with rather large value of A the measured current has bulk nature. Thus, in the below analysis only bulk carrier transport mechanisms are taken into account. Fig. 1 shows the reverse *I–U* characteristics within the temperature range 77…156 K. They are satisfactorily approximated by a power dependence $I \sim U^m$. As seen, at temperatures $T < 120$ K and reverse bias voltages $U \leq 0.2$ V the sublinear *I–U* dependences with the exponent $m \cong 0.8$ are observed. At higher temperatures (curves *4*, *5*), *I–U* characteristics change significantly. At the bias voltages $U \leq 0.03$ V, the exponent $m \cong 0.7…0.8$, whereas at $0.04 < U \leq 0.2$ V the reverse current tends to saturation and the exponent m equals approximately 0.3, which is typical for the thermal generation mechanism of carrier transport in homogeneous *p-n* junctions [1, 17]. With the reverse bias increase, the current gradually increases. The exponent m varies from 2 to 3 at $U = 1…2$ V up to 4.5…5.0 at higher biases, irrespective of temperature. In the case of the voltage breakdown in a *p-n* junction is determined at the current density equal to 1 A/cm^2 [18], in the investigated junctions the breakdown voltage U_B is decreased from 3 down to 1.8 V within the temperature range 77…156 K, which clearly indicates realization of tunnelling mechanism inherent to carrier transport [17].

The temperature dependences of the reverse current measured at several fixed values of the bias voltage are shown in Fig. 2 (curves *1-6*). At relatively small biases

© 2015, V. Lashkaryov Institute of Semiconductor Physics, National Academy of Sciences of Ukraine

Semiconductor Physics, Quantum Electronics & Optoelectronics, 2015. V. 18, N 3. P. 267-271.
doi: 10.15407/spqeo18.03.267

$U \leq 0.2$ V and temperatures higher than 120 K, the activation dependences are observed with the energy close to 0.13 eV, indicating thermal generation of carriers via deep defect states in the depletion region [1]. The presence of deep donor states with the activation energy 132 ± 3 meV and density 10^{13} cm^{-3} has been reported in [19]. In the authors opinion, these states were not associated with technology of the starting material. The lack of activation parts in *I–U* characteristics at the biases $U \geq 0.5$ V (curves *4-6*) is attributed to contribution of tunneling current component to the overall current.

In the case when the reverse current dominates over the interband tunneling, it is given by [17]:

$$I = \frac{\sqrt{2m^*}e^3 FUA}{4\pi^2 E_g^{1/2}} \exp\left(-\frac{4\sqrt{2m^*}E_g^{3/2}}{3eF\hbar}\right), \qquad (2)$$

where F is the electric field in the junction, A − junction area and other symbols have their usual meaning. Obviously, the temperature dependence of the interband tunneling current is determined mainly by the dependence of E_g on temperature. Shown in Fig. 3 are temperature dependences of the measured current plotted in $\lg I – E_g^{3/2}$ coordinates. The decrease in their slope at higher biases may be caused by the increased contribution of the interband tunneling current. At the reverse bias $U = 2$ V, this current seems to be dominant. By using the equation (2), one can estimate the breakdown voltage for the homogeneous junction, Fig. 4. As seen, there exist a large discrepancy between experimental and calculated values of the breakdown voltage (3 and 15 V, respectively). This means that another model of tunneling current should be invoked to interpret experimental data correctly.

In a number of published papers [20-26], various models of the tunneling current in the reverse biased diodes were developed. For instance, the interband tunneling current associated with dislocations has been analyzed in [20-22].

A model of the barrier width inhomogeneity has been proposed in [23]. Due to fluctuation of dopant concentration, the local thin barriers can dominate in the overall transport of carriers. A model of trap-assisted tunneling (TAT) current has been developed in [24, 25]. Based on this model experimental data were satisfactorily explained in $Cd_xHg_{1-x}Te$ (x = 0.2…0.3) [25] and InAs infrared photodiodes [26].

The excess tunneling current in the forward-biased InAs photodiodes was satisfactorily explained in terms of inhomogeneous junction that contains local areas with a much higher concentration of defects [26]. The local inhomogeneities may be related to dislocations or other extended defects that release excess strains in semiconductors. As known, dislocations can substantially affect distribution of dopant impurities because they provide a fast pathway to impurities as well as can segregate impurities. Due to the last reason, the so-called Cottrell atmospheres are formed around dislocations. Typical values of their diameter are of the order of 0.5…2 μm [2]. To explain the experimental data in Fig. 4, it was assumed that the area of a local inhomogeneity should correlate with the average diameter of Cottrell atmosphere. Thus, the total area of inhomogeneities A_1 should be proportional to the density of dislocation. At the same time, it is obvious that the area A_1 is much less (several orders of magnitude) than the junction area A. Taking this into account, the junction parameters determined from *C–U* measurements refer to the homogeneous part of the junction. The same parameters (a, W and F) for inhomogeneities can be determined from the

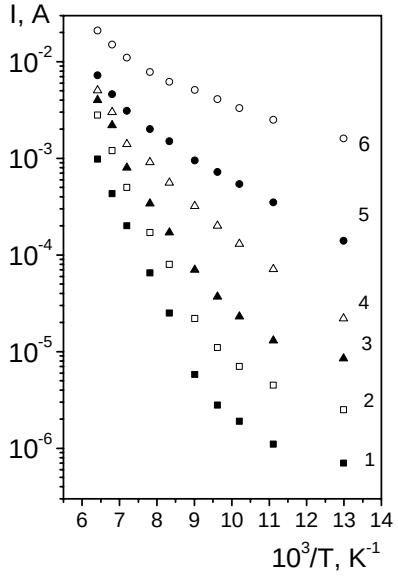

Fig. 2. Temperature dependences of reverse current at bias voltages, V: 0.01 (*1*), 0.05 (*2*), 0.2 (*3*), 0.5 (*4*), 1.0 (*5*), 2.0 (*6*).

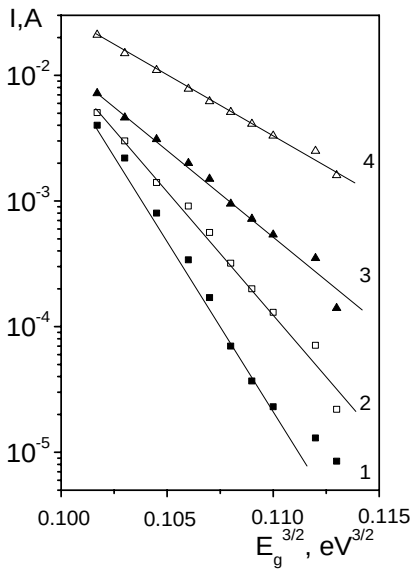

Fig. 3. Reverse current as a function of temperature dependence of the forbidden gap at bias voltages, V: 0.2 (*1*), 0.5 (*2*), 1 (*3*), 2 (*4*).

© 2015, V. Lashkaryov Institute of Semiconductor Physics, National Academy of Sciences of Ukraine

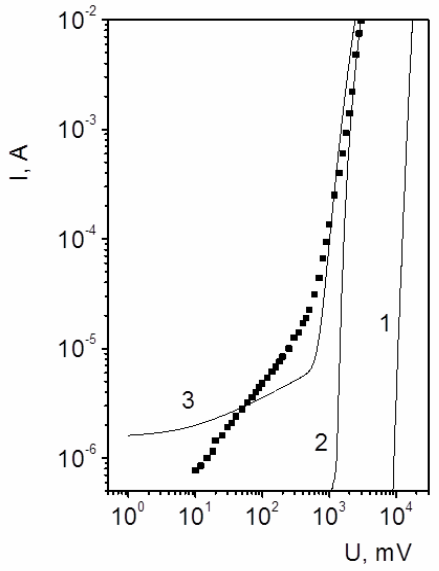

Fig. 4. Experimental (dots) and calculated (solid lines) reverse *I–U* characteristics at 77 K. The calculated curves refer to interband tunneling current via homogeneous region (1), interband tunneling current via local inhomogeneities (2), TAT current via local inhomogeneities including thermal and tunnel transitions (3). Parameters used for calculation: $a = 1.9\cdot10^{19}$ cm^{-4}, $m_e^* = 0.014m_0$, $m_h^* = 0.015m_0$, $A_1 = 2\cdot10^{-5}$ cm^2, $a_1 = 2.1\cdot10^{21}$ cm^{-4}, $E_t = E_g/2$, $N_t = 1\cdot10^{14}$ cm^{-3}, $\tau_1 = 10^{-9}$ s, $\varepsilon = 17$.

temperature dependences of the reverse current measured at high biases, which are assumed to be caused by interband tunneling with their participation. The following values were found from the dependences shown in Fig. 3 at the reverse voltage 2 V: $F_1 = 8.4\cdot10^4$ V/cm, $W_1 = 4.8\cdot10^{-5}$ cm and $a_1 = 2.1\cdot10^{21}$ cm^{-4}. These values are almost two orders of magnitude higher than those in the homogeneous part of the junction. From the fitting calculation (curve *2* in Fig. 4), the effective area of inhomogeneities of the order of 10^{-5} cm^2 was obtained. It must be pointed out that the calculations were performed for the maximum electric field $F_1 = 3(U + U_{bi})/2W_1$, where $W_1 = (12\varepsilon_0\varepsilon(U + U_{bi})/ea_1)^{1/3}$ is the depletion region width.

Concerning InSb photodiodes, a model of inhomogeneous junction has been successfully used for explanation of direct *I–U* characteristics [8]. It is natural to assume that the excess reverse current in the investigated junctions is also related to inhomogeneities. The TAT current is expressed as

$$I_{TAT} = eWN_tA\left(\frac{1}{\omega_v N_v + c_p p_1} + \frac{1}{\omega_c N_c + c_n n_1}\right)^{-1}, \quad (3)$$

where N_t is the density of traps participating in tunneling, $\omega_v N_v$ and $\omega_c N_c$ denote rates of tunneling transitions between the valence and conduction bands and traps in the gap, $c_p p_1$ and $c_n n_1$ are thermal transition rates [1].

The tunneling transition rates are given by

$$\omega_v N_v = \frac{\pi^2 e m_h F M^2}{h^3(E_g - E_t)}\exp\left[-\frac{4\sqrt{2m_h}(E_g - E_t)^{3/2}}{3e\hbar F}\right], \quad (4)$$

$$\omega_c N_c = \frac{\pi^2 e m_e F M^2}{h^3 E_t}\exp\left[-\frac{4\sqrt{2m_e}E_g^{3/2}}{3e\hbar F}\right], \quad (5)$$

where E_t is the trap energy measured from the conduction band edge, M – matrix element for tunneling transitions via traps [27]:

$$M = \frac{2\hbar^2\sqrt{2\pi}}{m_0}\left(\frac{2m_0}{\hbar^2}\right)^{1/4}\frac{E_g}{E_t^{1/4}}, \quad (6)$$

where m_0 is the free electron mass. It should be pointed out that this model has developed for homogeneous distribution of traps in the depletion region. Because of in InAs effective masses of electrons and light holes, m_e and m_h, are approximately equal, the tunneling probability reaches maximum for the midgap states $E_t = E_g/2$, for which $\omega_v N_v = \omega_c N_c$ and $(c_p p_1)^{-1} = (c_n n_1)^{-1} = \tau$. In the calculations, the effective lifetime τ served as an adjustable parameter. The used value of N_t correlates well with the concentration of deep centers found in [18, 28], but the generation lifetime is chosen to be one order of magnitude less than that in homogeneous InSb *p-n* junctions [1].

The calculated TAT current through the local inhomogeneities is shown in Fig. 4 (curves *2* and *3*). In the bias voltage range 0.8…2 V the calculated *I–U* dependence satisfactorily coincides with experimental data. At biases $U < 0.7$ V, thermal transitions are dominant (curve *3*), whereas within the range $0.7 < U < 2.0$ V the tunneling component of TAT current prevails. The difference between the slope of calculated and measured curves at $U < 0.7$ V may be caused by the dependence of the generation time τ on electric field in the depletion region or participation of several traps in the carrier transport. At biases $U \geq 2.0$ V, better coincidence of experimental and calculated *I–U* characteristics is observed for the interband tunneling current via local inhomogeneities (curve *2*). There is no need to prove that in this case the voltage breakdown strongly depends on availability of local inhomogeneities in the active region of *p-n* junctions and their parameters such as density and concentration gradient.

Thus, the excess tunneling current in the investigated diffused InSb *p-n* junctions at temperatures close to 77 K is explained by local inhomogeneities in the depletion region. At a relatively small bias voltages $eU < 2E_g$, thermal transitions via traps in the gap are dominant. In the bias voltage range $3E_g \leq eU \leq 8E_g$, the TAT current is dominant and at high biases $eU > 8E_g$ the current is determined by the interband tunnelling.

© 2015, V. Lashkaryov Institute of Semiconductor Physics, National Academy of Sciences of Ukraine

3. Conclusions

1. The carrier transport mechanisms are investigated in the linearly graded *p-n* junctions prepared by cadmium diffusion into *n*-InSb single crystal substrates. Experimental results are satisfactorily explained within the model of inhomogeneous *p-n* junction. The total dark current consists of generation and tunneling components. The excess tunneling current is caused by carrier transport via local inhomogeneities.
2. Dispersion of breakdown voltages in InSb photodiodes prepared by different methods is mostly caused by the interband tunneling current via local inhomogeneities.

References

1. A. Rogalskii (Ed.), *Infrared Photon Detectors*. SPIE Optical Eng. Press, 1995.
2. P.V. Birulin, V.I. Turinov, E.B. Yakimov, Characteristics of InSb photodiode linear arrays // *Semiconductors*, **38**(4), p. 488-503 (2004).
3. A.M. Filachev, I.D. Burlakov, A.I. Dirochka et al., Fast-operating array photodetective assembly of a 128×128 elements format on the basis of InSb with the frame-accurate accumulation and function of the range finder // *Prikladnaya Fizika*, No.2, p. 21-25 (2005), in Russian.
4. A. Rogalski, Optical detectors for focal plane arrays // *Opto-Electron. Rev*. **12**(2), p. 221-245 (2004).
5. E. Hurwitz, I.P. Donnely, Planar InSb photodiodes fabricated by Be and Mg implantation // *Solid State Electron.* **18** (9), p. 753-756 (1975).
6. V.P. Astahov, D.A. Gindin, V.V. Karpov et al., Developments in InSb-photodetectors with very-low-level dark current for use in high performance IR CCDs // *Prikladnaya Fizika*, No.2, p. 73-79 (1999), in Russian.
7. V.P. Astahov, D.A. Gindin, V.V. Karpov, A.V. Talimov, On the possibility of increasing the current sensitivity in InSb-based photodiodes // *Prikladnaya Fizika*, No.1, p. 56-62 (2002), in Russian.
8. A. Sukach, V. Tetyorkin, A. Voroschenko, A. Tkachuk et al., Carrier transport mechanisms in InSb diffusion *p-n* functions // *Semiconductor Physics, Quantum Electronics and Optoelectronics*, **17**(4), p. 325-330 (2014).
9. R.D. Thom, T.L. Hoch, I.D. Langan et al., A fully monolithic InSb infrared CCD array // *IEEE Trans. Electron. Dev.*, **ED-27**, p.160-170 (1980).
10. R. Adar, V. Nemirovsky and I. Kidron, Bulk tunneling contribution to the reverse breakdown characteristics of InSb gate controlled diodes // *Solid State Electron.* **30**(12), p.1289-1293 (1987).
11. S.L. Tu, K.F. Huang, InSb p-n function with avalanche breakdown behavior // *Jpn. J. Appl. Phys*. **28**(11), p. L1874-L1876 (1989).
12. H.A. Protschka, D.C. Shang, InSb photodiodes, with high reverse breakdown voltage // *International Electron Devices Meeting*, **13**, p. 56 (1967).
13. J. Abautret, J.P. Perez, A. Evirgen et al., Electrical modeling of InSb PiN photodiode for avalanche operation // *J. Appl. Phys*. **113**, p. 183716 (2013).
14. F. Dewald, The kinetics and mechanism of formation of anode films on single crystal InSb // *J. Electrochem. Soc*. **104**(4), p. 244-251 (1957).
15. M. Shroder, *Semiconductor Materials and Device Characterization*. Wiley, 2006.
16. Yu.F. Bikovskii, L.A. Vjukov, A.G. Dudoladov et al., Investigation of MIS film structures based on CdTe-InSb // *Pisma Zhurnal Tekhn. Fiziki*, **9**(17), p. 1071-1074 (1983), in Russian.
17 S.M. Sze, *Physics of Semiconductors Devices. Second Edition*, Wiley, 1981.
18. H.H. Smirnova, S.V. Slobodchikov, G.N. Talalakin, Reverse current and breakdown mechanisms in InAs // *Fizika Tekhnika Poluprovod.* **16**(12), p. 2116-2120 (1982), in Russian.
19. O.S. Shemelina, Yu.F. Novototskii-Vlasov, Equilibrium parameters of deep bulk levels in indium antimonide // *Fizika Tekhnika Poluprovod.* **26**(6), p. 1015-1023 (1992), in Russian.
20. V. Ravi, *Imperfections and Impurities in Semiconductor Silicon*. Wiley, 1981.
21. A.Ya. Vul', V.N. Koryayev, P.G. Petrosyan et al., p-n junctions in GaAs-GaSb solid solutions // *Fizika Tekhnika Poluprovod.* **16**(10), p. 1838-1842 (1982), in Russian.
22. A.Ya. Vul', T.A. Polanskaya, I.G Savelyev et al., On the mechanism of breakdown of p-n junctions based on $GaAs_{1-x}Sb_x$ solid solutions // *Fizika Tekhnika Poluprovod.* **17**(1), p. 134-138 (1983).
23. M.E. Raikh, I.M. Ruzin, Fluctuation mechanism of excess tunneling current in reverse-biased p-n junctions // *Fizika Tekhnika Poluprovod.* **19**(7), p. 1217-1225 (1985), in Russian.
24. W.W. Anderson and H.J. Hoffman, Field ionization of deep levels in semiconductors with application to $Hg_{1-x}Cd_xTe$ p-n junctions // *J. Appl. Phys*. **53**(12), p. 9130-9145 (1982).
25. Y. Nemirovsky, A. Unikovsky, Tunneling and 1/f noise currents in HgCdTe photodiodes // *J. Vac. Sci. Technol. B*, **10**(4), p. 1602-1610 (1992).
26. V. Tetyorkin, A. Sukach and A. Tkachuk, InAs infrared photodiodes, In: *Advances in Photodiode.* Ed. G.-F. Dalla Betta, InTech, p. 427-446(2011).
27. He Wenmu, Celik-Batler Zeynep, 1/f noise and dark current in HgCdTe components in HgCdTe MIS infrared detectors // *Solid State Electron.* **19**(1), p. 127-132 (1996).
28. G.J. Nott, P.C. Findlay, J.G. Crowder et al., Direct determination of Shockley-Read-Hall trap density in InSb/InAlSb detectors // *J. Phys. Condens. Matter*, **12**, p. L731-L734 (2000).

© 2015, V. Lashkaryov Institute of Semiconductor Physics, National Academy of Sciences of Ukraine